J Electroceram (2007) 18:205–218
DOI 10.1007/s10832-007-9024-7

Oxygen permeability, stability and electrochemical behavior of $Pr_2NiO_{4+\delta}$-based materials

A. V. Kovalevsky · V. V. Kharton · A. A. Yaremchenko · Y. V. Pivak · E. V. Tsipis · S. O. Yakovlev · A. A. Markov · E. N. Naumovich · J. R. Frade

Received: 29 May 2006 / Accepted: 17 October 2006 / Published online: 24 February 2007

Abstract The high-temperature electronic and ionic transport properties, thermal expansion and stability of dense $Pr_2NiO_{4+\delta}$, $Pr_2Ni_{0.9}Fe_{0.1}O_{4+\delta}$ and $Pr_2Ni_{0.8}Cu_{0.2}O_{4+\delta}$ ceramics have been appraised in comparison with K_2NiF_4-type lanthanum nickelate. Under oxidizing conditions, the extensive oxygen uptake at temperatures below 1073–1223 K leads to reversible decomposition of Pr_2NiO_4-based solid solutions into Ruddlesden–Popper type $Pr_4Ni_3O_{10}$ and praseodymium oxide phases. The substitution of nickel with copper decreases the oxygen content and phase transition temperature, whilst the incorporation of iron cations has opposite effects. Both types of doping tend to decrease stability in reducing atmospheres as estimated from the oxygen partial pressure dependencies of total conductivity and Seebeck coefficient. The steady-state oxygen permeability of $Pr_2NiO_{4+\delta}$ ceramics at 1173–1223 K, limited by both surface-exchange kinetics and bulk ionic conduction, is similar to that of $La_2NiO_{4+\delta}$. The phase transformation on cooling results in considerably higher electronic conductivity and oxygen permeation, but is associated also with significant volume changes revealed by dilatometry. At 973–1073 K, porous $Pr_2Ni_{0.8}Cu_{0.2}O_{4+\delta}$ electrodes deposited onto lanthanum gallate-based solid electrolyte exhibit lower anodic overpotentials compared to $La_2Ni_{0.8}Cu_{0.2}O_{4+\delta}$, whilst cathodic reduction decreases their performance.

Keywords Praseodymium nickelate · Mixed ionic–electronic conductor · Oxygen permeation · Thermal expansion · SOFC cathode

A. V. Kovalevsky · V. V. Kharton (✉) · A. A. Yaremchenko · Y. V. Pivak · E. V. Tsipis · S. O. Yakovlev · E. N. Naumovich · J. R. Frade
Department of Ceramics and Glass Engineering, CICECO, University of Aveiro, 3810-193 Aveiro, Portugal
e-mail: kharton@cv.ua.pt

V. V. Kharton · E. N. Naumovich
Institute of Physicochemical Problems, Belarus State University, 14 Leningradskaya Str., 220050 Minsk, Belarus

A. A. Markov
Institute of Solid State Chemistry, Ural Division of RAS, 91 Pervomayskaya Str., Ekaterinburg 620219, Russia

1 Introduction

Solid solutions based on rare-earth nickelates with K_2NiF_4-type structure, $A_2NiO_{4\pm\delta}$, are a promising group of mixed-conducting materials with potential applications for the cathodes of intermediate-temperature solid oxide fuel cells (IT SOFCs) and oxygen-separation membranes [1–11]. For these systems, the maximum emphasis in literature was focused on lanthanum nickelate, $La_2NiO_{4+\delta}$. Important advantages of La_2NiO_4-based compositions include a relatively high level of oxygen-ionic and p-type electronic transport, moderate thermal and chemical expansion, and a significant electrocatalytic activity under oxidizing conditions. The oxygen permeation through dense lanthanum nickelate membranes is essentially limited by kinetics of redox processes at the surface [1, 3]; this prevents bulk decomposition and enables stable operation under air/CH_4 gradients up to temperatures as high as 1150–1170 K [12]. Also, partial reduction of the membrane surface exposed to reducing atmosphere results in formation of porous La_2O_3-supported Ni catalyst layer, which may provide a high selectivity towards partial oxidation of methane [8]. The crystal structure of $La_2NiO_{4+\delta}$ is built of alternating rock-salt La_2O_2 and perovskite NiO_2 layers, and can accommodate a significant oxygen excess. The extra O^{2-} anions,

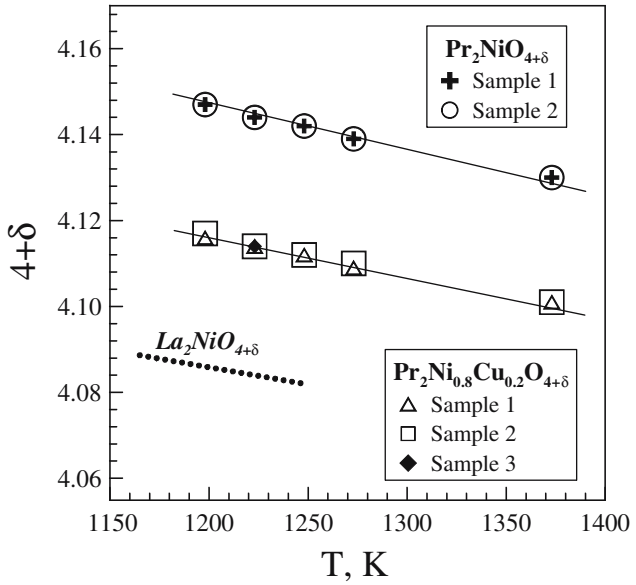

Fig. 1 Total oxygen content in $Pr_2NiO_{4+\delta}$ and $Pr_2Ni_{0.8}Cu_{0.2}O_{4+\delta}$ at atmospheric oxygen pressure, determined by TGA. The reproducibility error is ±0.001. The data on $La_2NiO_{4+\delta}$ [16] are shown for comparison

charge-compensated by electron holes localized on nickel cations, occupy interstitial positions in the LaO bilayers [4, 10]. The equilibrium oxygen hyperstoichiometry (δ) in air is close to 0.14–0.15 at 300 K and decreases on heating [2, 6]. The ionic transport occurs via a complex mechanism involving diffusion of interstitial oxygen ions in the rock-salt layers and oxygen vacancies in the perovskite planes.

$Pr_2NiO_{4+\delta}$ exhibits a larger range of the oxygen nonstoichiometry variations compared to lanthanum nickelate [13], due to smaller size of the A-site cations and, possibly, to the presence of a minor fraction of tetravalent Pr^{4+}. The effects of A-site cation radius on the oxygen transport properties are, however, still unclear. In the case of isostructural cuprates, $Ln_2CuO_{4+\delta}$ (Ln=La, Pr, Nd), the ionic conduction was found to decrease with decreasing rare-earth cation size as La>Pr>Nd [3]. A similar tendency, known also for perovskite-type cobaltites, was observed when substituting 50% lanthanum cations in $La_2NiO_{4+\delta}$ with praseodymium [3]. On the contrary, $Pr_2NiO_{4+\delta}$ was reported to exhibit the highest oxygen tracer diffusion coefficients in $Ln_2NiO_{4+\delta}$ series [5]. These contradictions may result from thermodynamic metastability of the K_2NiF_4-type praseodymium nickelate phase at temperatures below 1123 K in oxidizing atmospheres, where $Pr_2NiO_{4+\delta}$ decomposes into the Ruddlesden–Popper type $Pr_4Ni_3O_{10}$ and Pr_6O_{11} [7]. Note that the segregation of praseodymium oxide, having a high catalytic activity in electrochemical reactions involving gaseous oxygen, may be advantageous for the SOFC cathode applications [10]. For example, the deposition of PrO_x onto $La_2Ni_{0.8}Cu_{0.2}O_{4+\delta}$ electrodes in contact with $(La_{0.9}Sr_{0.1})_{0.98}Ga_{0.8}Mg_{0.2}O_{3-\delta}$ (LSGM) solid electrolyte made it possible to decrease cathodic overpotentials by 1.5–2 times [10].

The present work was centered on the analysis of oxygen permeability, electronic conductivity and thermal expansion of $Pr_2NiO_{4+\delta}$ ceramics in the vicinity of phase

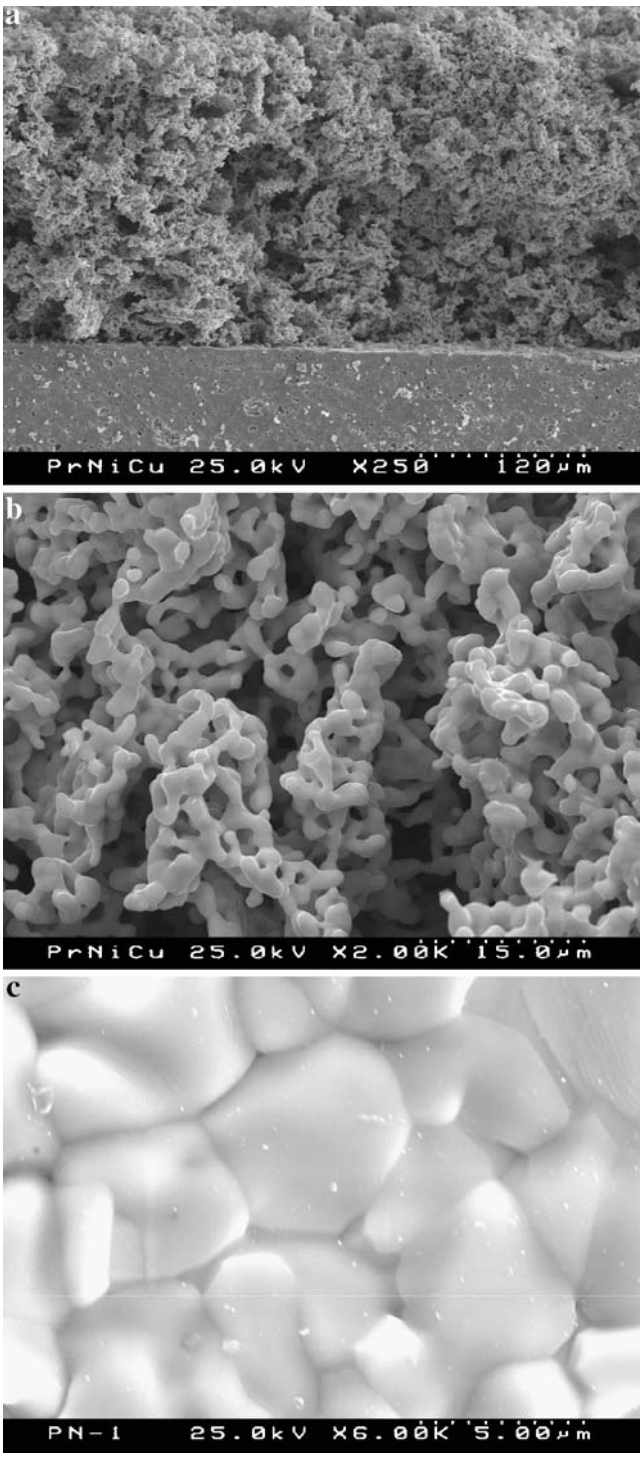

Fig. 2 SEM micrographs of fractured electrochemical cells with $Pr_2Ni_{0.8}Cu_{0.2}O_4$ cathode applied onto LSGM electrolyte after the polarization measurements (**a** and **b**), and fractured $Pr_2NiO_{4+\delta}$ ceramics (**c**)

Table 1 Properties of as-prepared nickelate ceramics.

Material	Phase composition (space group)	Unit cell parameters, Å	Average thermal expansion coeffcients	
			T, K	$\overline{\alpha} \times 10^{-6}$, K^{-1}
$Pr_2NiO_{4+\delta}$	Orthorombic (*Bmab*)	a=5.3934(1)	300–970	13.11±0.01
		b=5.4564(1)	970–1220	20.11±0.07
		c=12.4479(2)	1320–1470	13.26±0.07
$Pr_2Ni_{0.9}Fe_{0.1}O_{4+\delta}$	Orthorombic (*Bmab*)	a=5.4082(2)	300–970	13.55±0.01
		b=5.4708(2)	970–1300	16.66±0.01
		c=12.4343(4)	1300–1335	13.03±0.03
$Pr_2Ni_{0.8}Cu_{0.2}O_{4+\delta}$	Tetragonal (*P4$_2$/ncm*) (83.8 wt.%)	a=5.4307(4)	300–1030	13.24±0.01
		c=12.5230(12)	1030–1150	17.49±0.04
			1210–1280	12.89±0.01
	Orthorhombic(*Bmab*) (13.5 wt.%)	a=5.383(1)		
		b=5.4744(15)		
		c=12.5323(40)		
$La_2NiO_{4+\delta}$	Tetragonal *(I4/mmm)*	a=3.86464(8)	400–1290	13.59±0.01
		c=12.6914(3)		

boundary. Two derivatives of praseodymium nickelate, namely $Pr_2Ni_{0.9}Fe_{0.1}O_{4+\delta}$ and $Pr_2Ni_{0.8}Cu_{0.2}O_{4+\delta}$, were also studied in order to access the influence of higher- and lower-valence dopants, in comparison with the La-containing analogues [3, 10]. For the evaluation of electrochemical performance, porous $Pr_2Ni_{0.8}Cu_{0.2}O_{4+\delta}$ layers applied onto LSGM electrolyte were tested under conditions similar to those used in previous studies of $La_2Ni_{0.8}Cu_{0.2}O_{4+\delta}$ [10].

2 Experimental

Powders of $Pr_2NiO_{4+\delta}$, $Pr_2Ni_{0.9}Fe_{0.1}O_{4+\delta}$, $Pr_2Ni_{0.8}Cu_{0.2}O_{4+\delta}$ and $La_2NiO_{4+\delta}$ were prepared via glycine-nitrate process (GNP), a self-combustion technique using nitrates of metal components as an oxidant and glycine as a fuel and chelating agent [14]. In the course of synthesis, glycine was added into aqueous solutions containing Pr, Ni, Fe, Cu or La nitrates in the stoichiometric proportion. The molar glycine/nitrate ratio was twice of stoichiometric, calculated assuming that the only gaseous products of the reaction are N_2, H_2 and CO_2. After drying and autoignition, the resultant powder was calcined in air at 1200–1350 K for 2 h in order to remove organic residues, ball-milled and pressed into disks. Ceramic samples with 95–98% density were sintered in air at 1573–1673 K for 3–5 h and cooled down with a rate of 3–4 K/min. These samples, hereafter called "as-prepared," were used for the measurements of electrical conductivity, Seebeck coefficient and oxygen permeability, and for dilatometric studies. Since the achievement of equilibrium phase composition in dense ceramics is often kinetically stagnated as shown below, a series of $Pr_2NiO_{4+\delta}$, $Pr_2Ni_{0.9}Fe_{0.1}O_{4+\delta}$ and $Pr_2Ni_{0.8}Cu_{0.2}O_{4+\delta}$ samples were annealed in air at 1223 K (24 h) or at 1073 K (50 h), or in flowing argon at $p(O_2)\approx 10^{-5}$ atm and at 1223 K (43 h), with subsequent quenching in liquid nitrogen and X-ray diffraction (XRD) analysis.

The XRD patterns were collected at room temperature using a Rigaku D/MAX-B diffractometer (CuK_α, 2Θ=10–100°, step 0.02°, 1 s/step); the structural parameters were refined employing the Fullprof program [15]. In the course of refinement, the scale factor, zero shift, background and unit-cell parameters, atomic coordinates and fractions, isotropic temperature factors, and the peak profile and texture parameters were calculated; the background was described using a linear interpolation. The choice of space

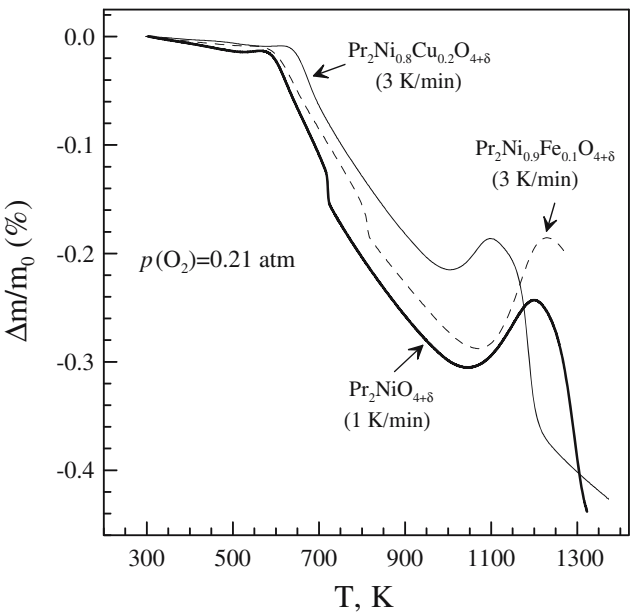

Fig. 3 Relative weight changes of as-prepared $Pr_2NiO_{4+\delta}$, $Pr_2Ni_{0.8}Cu_{0.2}O_{4+\delta}$ and $Pr_2Ni_{0.9}Fe_{0.1}O_{4+\delta}$, observed in the regime of continuous heating in air

groups was based on the analysis of systematic absence of reflexes. The orthorhombic *Fmmm* and *Bmab*, and tetragonal $P4_2/ncm$ and *I4/mmm* space groups were tested; final selection was based on the agreement factors. Thermal expansion in air was studied using a vertical alumina Linseis L75V/1250 dilatometer; all dilatometric data presented in this work correspond to the heating regime (3 K/min). A Hitachi S-4100 scanning electron microscope (SEM) with a Rontec UHV Detection system for the energy dispersive spectroscopy (EDS) was used for microstructural studies. The changes in oxygen content were determined by thermogravimetric analysis (TGA) using a Setaram SetSys 16/18 instrument. The standard TGA procedure included heating up to 1223 K in flowing dry air, temperature cycling in the range 973–1223 K with the step of 50 K and equilibration at each temperature during 2–10 h, flushing the apparatus with argon, and then reduction in a 10% H_2–90% N_2 flow at 1223 K. Each TGA measurement was repeated for two to three powdered samples; the difference between δ values measured at 1173–1373 K was lower than 0.001 (Fig. 1).

The total conductivity (σ, four-probe DC) and Seebeck coefficient (α) were measured as functions of the oxygen partial pressure varying in the range from 10^{-15} atm to 0.5 atm at 973–1223 K, and also separately at 300–1373 K in atmospheric air. The isothermal measurements vs. $p(O_2)$ were performed simultaneously on two bar-shaped ceramic samples placed in an yttria-stabilized zirconia (YSZ) cell comprising an electrochemical oxygen pump and a sensor, separated by glass-ceramic sealant; the experimental technique was described elsewhere [17]. The criteria for equilibration after a change in either oxygen pressure or temperature included the relaxation rates of the conductivity and Seebeck coefficients less than 0.05%/min and 0.001 μV/(K×min), respectively. The conductivity measurements in air were performed after equilibration at

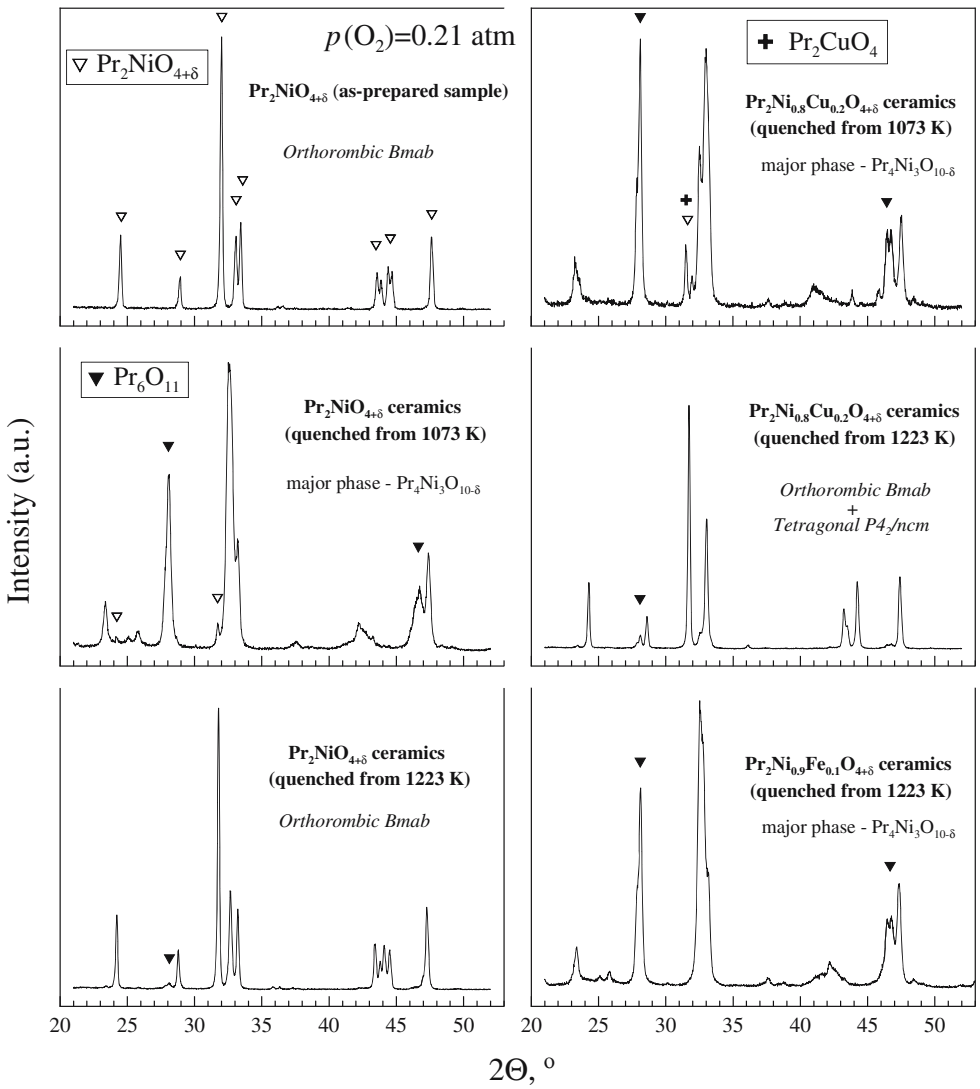

Fig. 4 XRD patterns of Pr_2NiO_4-based materials, quenched after annealing in air at 1073 K for 50 h and 1223 K for 24 h (see text). The pattern of as-prepared $Pr_2NiO_{4+\delta}$ (orthorhombic; S.G. *Bmab*) is given for comparison. In the cases when $Pr_4Ni_3O_{10}$-based solid solutions are the major phases, all unmarked peaks correspond to these phases

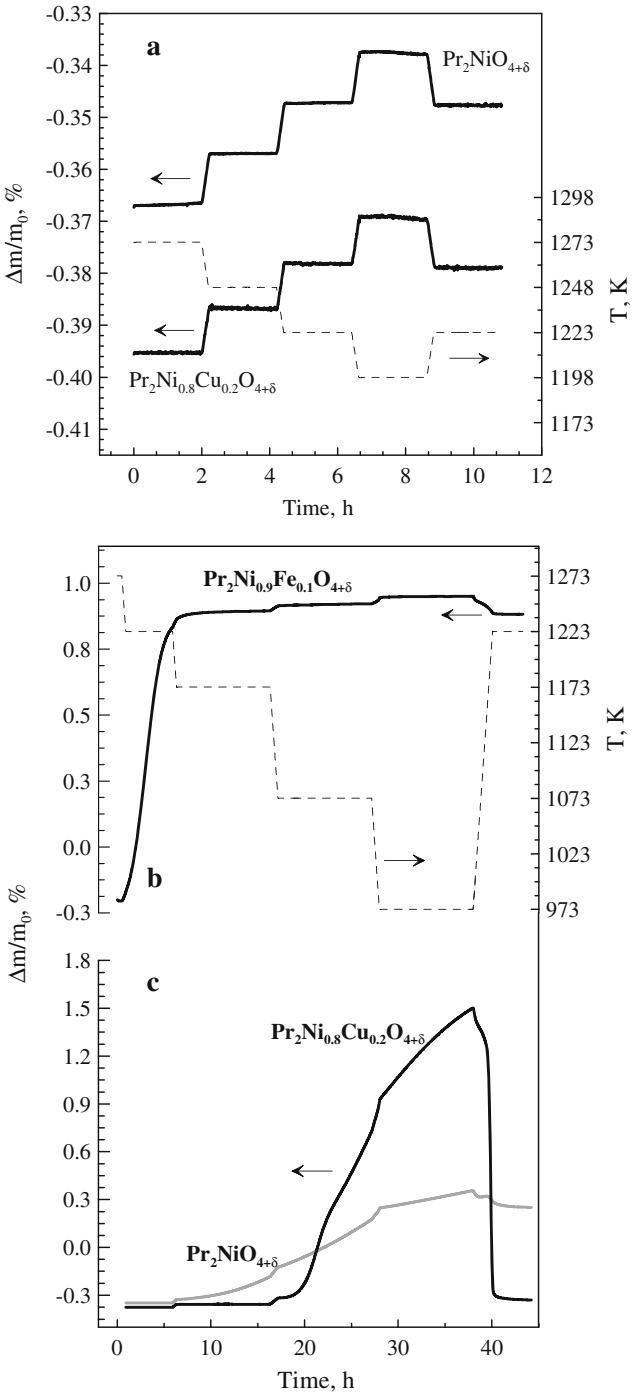

Fig. 5 Relative weight changes of powdered Pr_2NiO_4-based materials during isothermal steps in air. For **c**, the variations of temperature are identical to those shown in (**b**)

1270–1350 K, decreasing temperature by steps of 20–50 K. The relaxation time varied in the range 2–80 h.

The technique to study oxygen permeation using a solid-electrolyte cell with an oxygen pump and sensor was also described in previous work [18]. In terms of thermal pre-history of the membranes, the procedure included heating (3 K/min) up to softening of a glass sealant (1388 K), dwell for 5 min, and cooling down to 1223 K when the isothermal measurements were started. The oxygen partial pressure at the membrane permeate side (p_1) was varied in the range 1.5×10^{-2} to 0.20 atm; the feed-side oxygen pressure (p_2) was kept constant, 0.21 atm. Experimental procedure included temperature cycling in the range 1023–1223 K, with steps of 50 K and equilibration at each temperature. The criterion for a steady-state achievement was formulated as independence of the sensor e.m.f. on time during 10 h, with an accuracy of 0.5–0.7%; the transient times varied in the range 3 to 350 h. After the determination of oxygen fluxes at 1073–1223 K, all measurements were repeated two to four times in order to check reproducibility. For $Pr_2NiO_{4+\delta}$ membranes, the reproducibility error at temperatures far enough from the phase transition, such as 1223 or 1073 K, was 5–7%. In the vicinity of phase transformation, temperature cycling resulted in a higher error, 20–30%.

For the studies of electrode performance, porous layers of GNP-synthesized $Pr_2Ni_{0.8}Cu_{0.2}O_{4+\delta}$ were applied onto the surface of $(La_{0.9}Sr_{0.1})_{0.98}Ga_{0.8}Mg_{0.2}O_{3-\delta}$ (LSGM) solid electrolyte and fired in air at 1473 K for 2 h. The microstructure of resultant electrodes (thickness of approx.

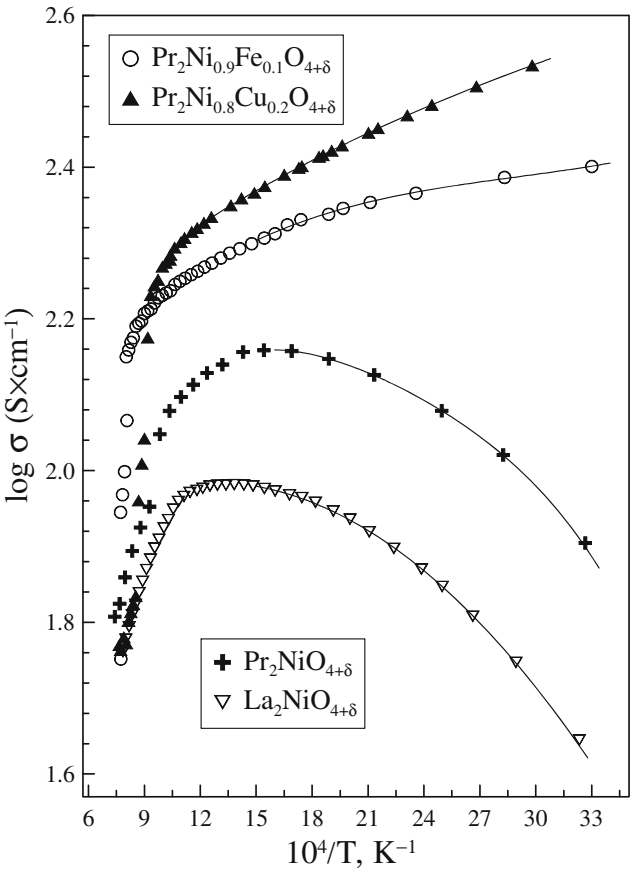

Fig. 6 Temperature dependence of the total conductivity of Pr_2NiO_4-based ceramics in air

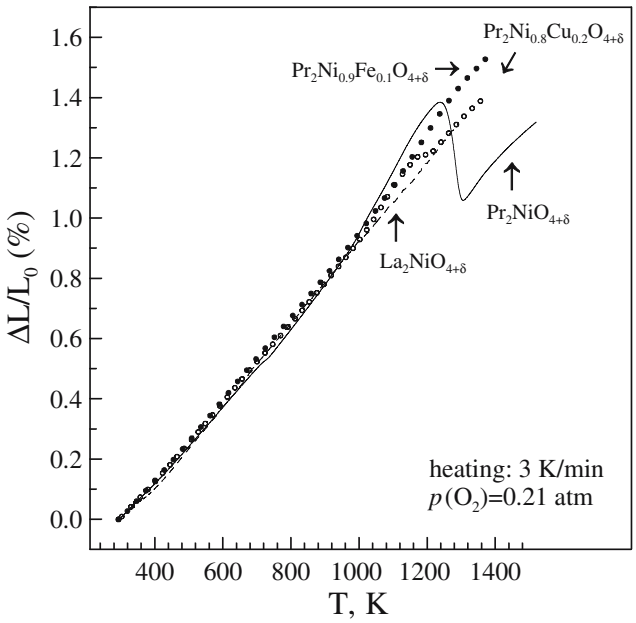

Fig. 7 Typical dilatometric curves of Pr_2NiO_4-based ceramics on heating in air

200 μm, sheet density of 17.8±0.6 mg/cm^2) is illustrated in Fig. 2a and b. The counter and reference electrodes were made of porous platinum. Testing of three-electrode cells with symmetrical location of the working and counter electrodes were performed at 873–1073 K in air, as described elsewhere [10, 19]. The ohmic resistance of the cell and the electrode polarization resistance (R_η) were determined from the impedance spectra collected in the frequency range from 10 mHz to 50 kHz.

3 Results and discussion

3.1 General characterization of ceramic materials

XRD analysis of the as-prepared materials showed the formation of single K_2NiF_4-type phases for all compositions, except for $Pr_2Ni_{0.8}Cu_{0.2}O_{4+\delta}$; the space groups (S. G.) and unit cell parameters are listed in Table 1. These structural data are all in agreement with literature [2, 5, 13, 20]. The as-prepared $Pr_2Ni_{0.8}Cu_{0.2}O_{4+\delta}$ ceramics consisted of two K_2NiF_4-type phases having the orthorhombic and tetragonal structures (Table 1). A similar phase separation is known for $Pr_2NiO_{4+\delta}$ with a reduced level

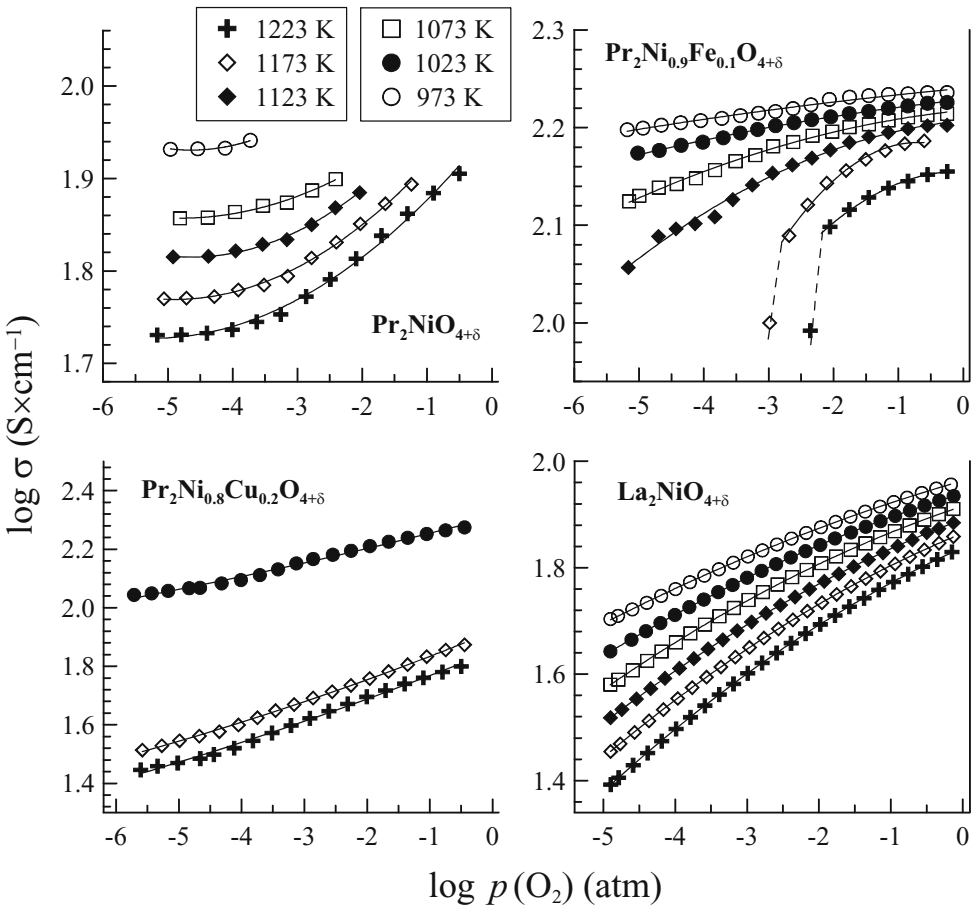

Fig. 8 Oxygen partial pressure dependence of the total conductivity under oxidizing conditions

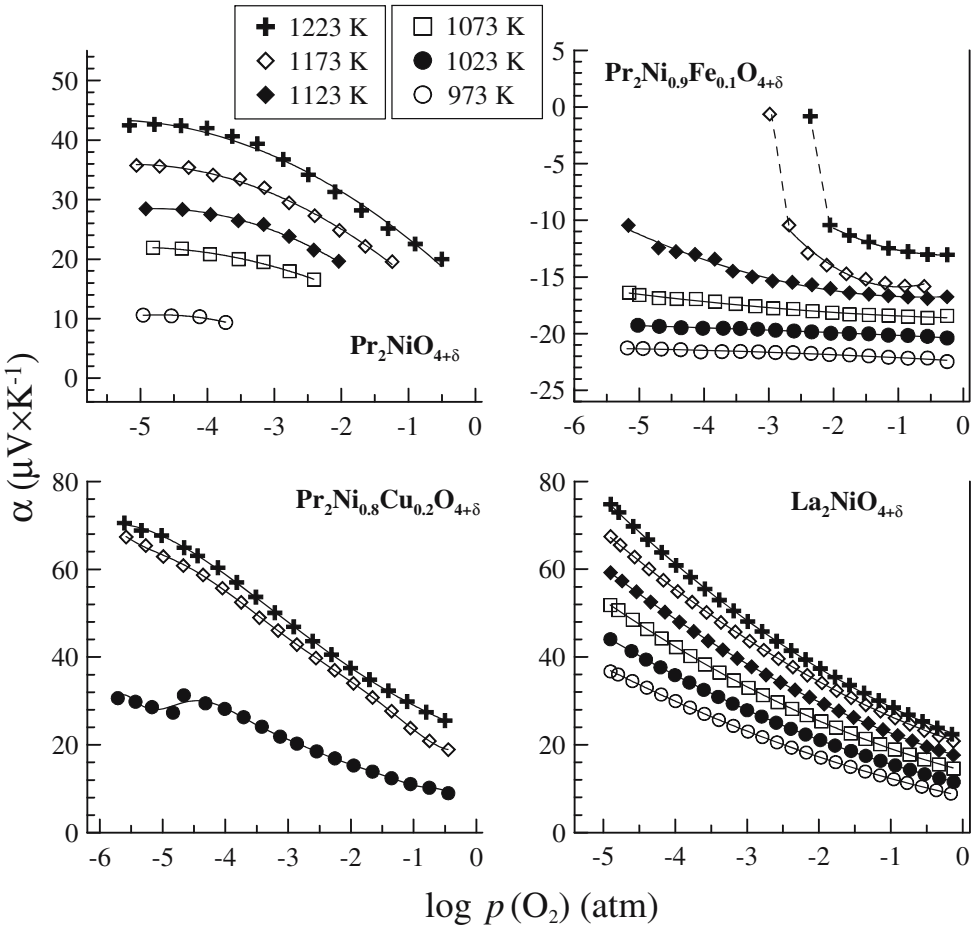

Fig. 9 Oxygen partial pressure dependence of Seebeck coefficient under oxidizing conditions

of oxygen hyperstoichiometry (δ=0.02–0.09) at 300 K [13, 21]. In the case of $Pr_2Ni_{0.8}Cu_{0.2}O_{4+\delta}$, this effect may also result from a lower oxygen content compared to undoped $Pr_2NiO_{4+\delta}$ (Fig. 1). SEM inspections revealed similar microstructures for all as-prepared ceramics; one typical SEM micrograph is presented in Fig. 2c. The average grain size was 3–7 μm.

The TGA data obtained on heating of as-prepared materials in air (Fig. 3), confirmed metastability of Pr_2NiO_4-based solid solutions at low temperatures, as for undoped praseodymium nickelate [7]. In the case $Pr_2Ni_{0.8}Cu_{0.2}O_{4+\delta}$, an extensive oxygen uptake starts at 970–1000 K; heating above 1100 K leads to drastic weight losses. The same processes are observed for $Pr_2NiO_{4+\delta}$ and $Pr_2Ni_{0.9}Fe_{0.1}O_{4+\delta}$ at slightly higher temperatures. For pure $Pr_2NiO_{4+\delta}$ in oxygen atmosphere [7], such behavior was attributed to the oxidative phase decomposition at temperatures above 1123 K, accompanied with an increase in the average oxidation state of nickel cations:

$$3Pr_2NiO_{4+\delta} + (1 - x + 2y - 3\delta)O_2 \rightarrow Pr_4Ni_3O_{10-x} + 2PrO_{1.5+y} \quad (1)$$

and the backward reaction on further heating. The same processes occur for all Pr_2NiO_4-based materials in air (Fig. 3). In other words, $Pr_2NiO_{4+\delta}$ and its derivatives are thermodynamically unstable at low temperatures, and start to extensively absorb oxygen and decompose at temperatures when the cation diffusion becomes significant. An opposite process is observed at high temperatures, when Pr_2NiO_4-based phases are formed again. tThis mechanism was validated by XRD analysis; selected XRD patterns are presented in Fig. 4. After annealing at 1073 K and quenching, the major phases in all Pr_2NiO_4-based materials were identified as praseodymium oxide and $Pr_4Ni_3O_{10}$-based solid solutions; an admixture of $Pr_2CuO_{4+\delta}$ was also found in the patterns of $Pr_2Ni_{0.8}Cu_{0.2}O_{4+\delta}$. After annealing of $Pr_2NiO_{4+\delta}$ and $Pr_2Ni_{0.8}Cu_{0.2}O_{4+\delta}$ at 1223 K in air, the formation of K_2NiF_4-type phases is observed again. These two materials became almost single-phase; the presence of minor Pr_6O_{11} impurities (Fig. 4) is associated with kinetically stagnated phase changes due to relatively slow cation diffusion. XRD inspections of $Pr_2Ni_{0.9}Fe_{0.1}O_{4+\delta}$ quenched after annealing at 1223 K in air, showed that $Pr_4(Ni,Fe)_3O_{10}$-based solid solution is still a major phase (Fig. 4). Therefore, the incorporation of

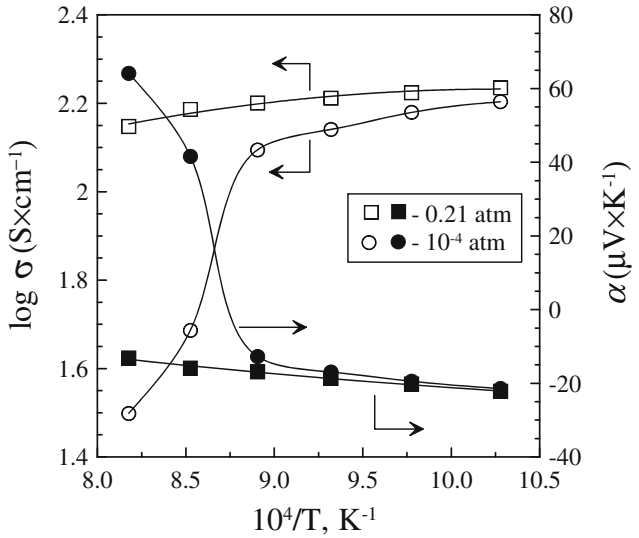

Fig. 10 Temperature dependencies of total conductivity and Seebeck coefficient of $Pr_2Ni_{0.9}Fe_{0.1}O_{4+\delta}$ ceramics at atmospheric oxygen pressure and at $p(O_2) = 1 \times 10^{-4}$ atm

copper cations decreases oxygen content and expands the stability domain of the K_2NiF_4-type solid solution towards lower temperatures, whereas iron doping has opposite effects. Such a behavior is well predictable, since the average oxidation state of transition metals cations in the K_2NiF_4-type lattices and, hence, oxygen content at a given $p(O_2)$ increase usually as Cu<Ni<Fe [3, 16].

These conclusions were further confirmed by the isothermal TGA tests, Fig. 5. The weight changes of powdered $Pr_2NiO_{4+\delta}$ and $Pr_2Ni_{0.8}Cu_{0.2}O_{4+\delta}$ exhibit a good reproducibility and fast equilibration on cycling at 1198–1223 K (Fig. 5a). At lower temperatures, prolonged transient processes start at 1173 K for undoped praseodymium nickelate, and at 1073 K for $Pr_2Ni_{0.8}Cu_{0.2}O_{4+\delta}$. The decomposition of $Pr_2Ni_{0.9}Fe_{0.1}O_{4+\delta}$ starts immediately upon cooling down to 1223 K.

3.2 Electrical conductivity and thermal expansion in air

Temperature dependencies of the total conductivity of Pr_2NiO_4-based ceramics in air are shown in Fig. 6. As for all other data on the electrical and electrochemical properties summarized in this work, these results correspond to the phase composition equilibrated with atmosphere. Prior to the measurements, all samples were kept in air at 1300 K for 20–25 h; the conductivity measurement were performed on cooling, with an equilibration at each temperature during 4–80 h.

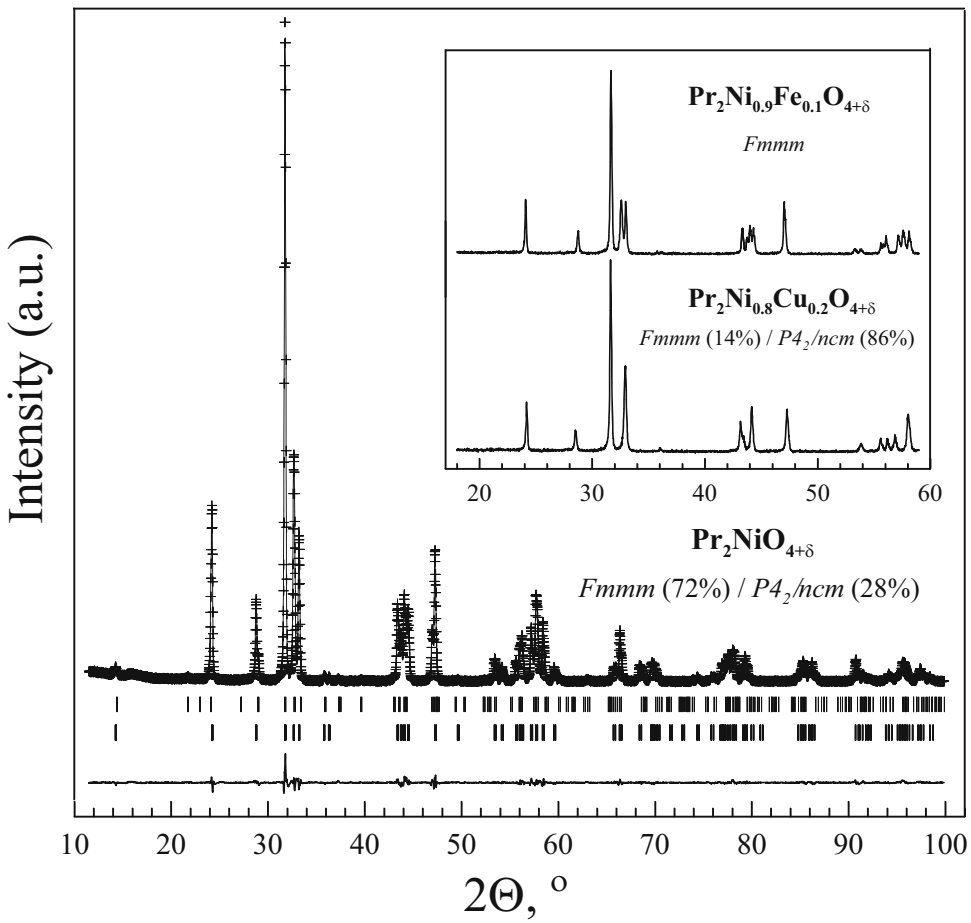

Fig. 11 Observed, calculated and difference XRD patterns of $Pr_2NiO_{4+\delta}$ after annealing at 1223 K in argon atmosphere and subsequent quenching. The refinement shows a mixture of orthorhombic (S.G. *Fmmm*) and tetragonal (S.G. *P4₂/ncm*) phases; the agreement factors R_p and R_{wp} are 5.2 and 6.9%, respectively. The *inset* shows the XRD patterns of $Pr_2Ni_{0.9}Fe_{0.1}O_{4+\delta}$ and $Pr_2Ni_{0.8}Cu_{0.2}O_{4+\delta}$ with similar pre-history. The refined space groups and estimated weight fractions of the K_2NiF_4-type phases with different symmetry are given in the legends

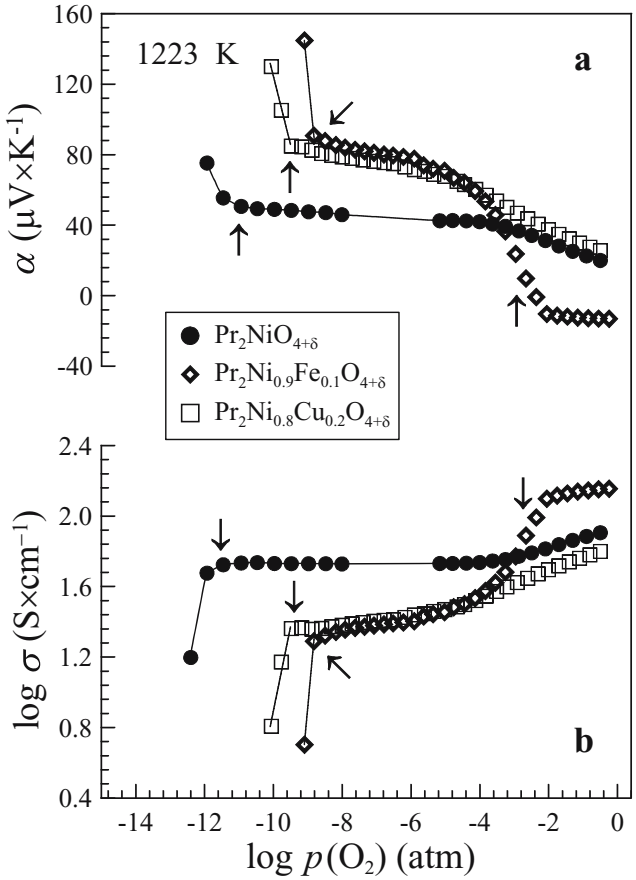

Fig. 12 Oxygen partial pressure dependencies of the Seebeck coefficient (**a**) and total conductivity (**b**) at 1223 K. The arrows show approximate limits of the K_2NiF_4-type phase existence domains

Within the stability domains of K_2NiF_4-type phases at temperatures above 1100–1200 K in air, all Pr-containing materials possess the total conductivity values close to $La_2NiO_{4+\delta}$ (Fig. 6). This suggests similar mechanisms of the conductivity, predominantly p-type electronic [2–6]. A slightly higher conductivity level in $Pr_2NiO_{4+\delta}$ with respect to lanthanum nickelate may be associated with higher oxygen content and hole concentration in the former compound (Fig. 1); any significant contribution of Pr^{4+}cations seems unlikely [22, 23]. When temperature decreases, phase transformation leads to a drastic increase of the σ values due to the formation of $Pr_4Ni_3O_{10}$-based solid solutions (Fig. 6). $Pr_4Ni_3O_{10-\delta}$ is known to exhibit a high, metallic-type conduction down to 4 K [24–26]. At temperatures below 800 K, the maximum conductivity is observed for $Pr_2Ni_{0.8}Cu_{0.2}O_{4+\delta}$ ceramics.

Figure 7 presents typical dilatometric curves of the as-prepared (metastable) ceramic materials, on heating in air. As for the conductivity, a clear correlation with TGA data is observed, within the limits of experimental uncertainties associated with stagnated kinetics of the phase changes. At 300–1000 K, Pr_2NiO_4-based ceramics show an almost linear expansion similar to that of $La_2NiO_{4+\delta}$; the apparent thermal expansion coefficients (TECs) lie in the range $(13.1–13.6)\times10^{-6}$ K^{-1}, Table 1. The oxygen uptake and partial phase decomposition of Pr_2NiO_4-based solid solutions above 970–1000 K are accompanied with the volume expansion; the reverse transition on further heating results in a sharp contraction. Due to the kinetic reasons, the latter process is invisible in the dilatometric curve of $Pr_2Ni_{0.9}Fe_{0.1}O_{4+\delta}$ ceramics where the transition into K_2NiF_4-type phase occurs at temperatures close to the upper temperature limit of the dilatometric measurements. At temperatures above phase transition, the dilatometric curves become, again, almost linear; the average TEC values are close to the low-temperature values, namely $(12.9–13.3)\times10^{-6}$ K^{-1} (Table 1). The dramatic volume changes of praseodymium nickelate ceramics, caused by the phase transformations, may lead to their mechanical incompatibility with other materials and, thus, limit their applications in electrochemical devices.

3.3 Phase composition and electrical properties vs. oxygen pressure

Selected $p(O_2)$-dependencies of the total conductivity and Seebeck coefficient under oxidizing conditions are shown in Figs. 8 and 9. For $Pr_2NiO_{4+\delta}$, these data correspond to domain where the single K_2NiF_4-type phase exists. The phase transition observed on decreasing temperature and increasing oxygen partial pressure, results in a substantially

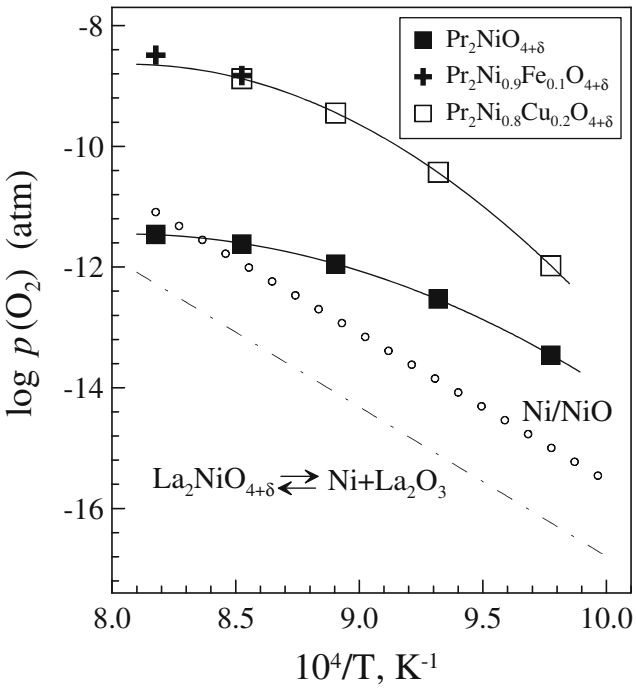

Fig. 13 Low-$p(O_2)$ stability limits of Pr_2NiO_4-based materials, estimated from the $p(O_2)$-dependencies of electrical properties. Data on Ni/NiO phase boundary [30] and $La_2NiO_{4+\delta}$ [28] are shown for comparison

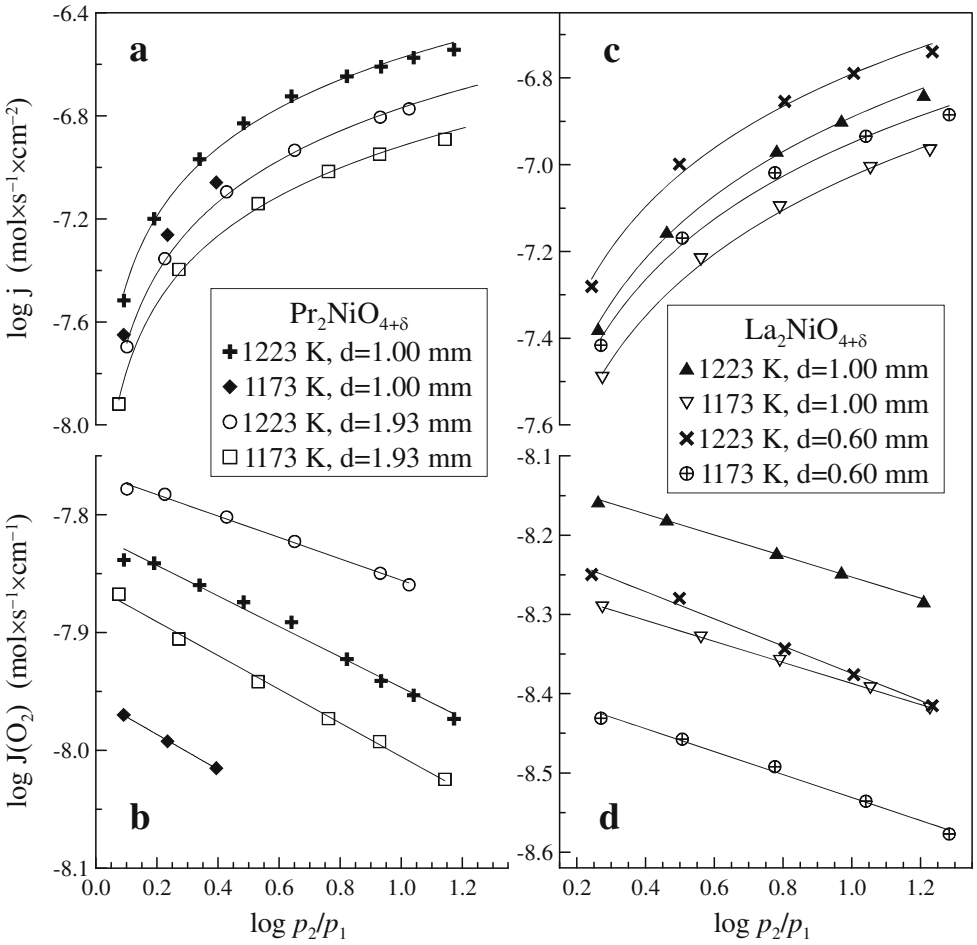

Fig. 14 Oxygen permeation fluxes (**a**, **c**) and specific oxygen permeability (**b**, **d**) of as-prepared $Pr_2NiO_{4+\delta}$ (**a**, **b**) and $La_2NiO_{4+\delta}$ (**c**, **d**) ceramic membranes at 1173–1223 K

higher conductivity, whilst the Seebeck coefficient decreases as illustrated by the example of $Pr_2Ni_{0.8}Cu_{0.2}O_{4+\delta}$. The variations of praseodymium nickelate electrical properties reveal the trends typical for p-type electronic conductors, although the observed behavior is considerably different with respect to $La_2NiO_{4+\delta}$.

In contrast, no single K_2NiF_4-type phase exists in $Pr_2Ni_{0.9}Fe_{0.1}O_{4+\delta}$ ceramics at 973–1223 K and oxygen pressures close to atmospheric, when this composition exhibits a negative thermopower and the conductivity values higher than 10^2 S/cm. The transition into K_2NiF_4 phase is only observed at 1173–1223 K and $p(O_2)<10^{-3}$–10^{-2} atm; the corresponding changes of the electrical properties are illustrated in Fig. 10. As an example, Fig. 11 presents the XRD patterns of Pr_2NiO_4-based materials quenched after annealing at 1223 K and $p(O_2)\approx10^{-5}$ atm during 43 h. In the cases of $Pr_2NiO_{4+\delta}$ and $Pr_2Ni_{0.8}Cu_{0.2}O_{4+\delta}$, mixtures of two K_2NiF_4-type phases were formed; $Pr_2Ni_{0.9}Fe_{0.1}O_{4+\delta}$ was found single-phase with an orthorhombic K_2NiF_4-like lattice. Notice that, although the symmetry of orthorhombic $Pr_2NiO_{4+\delta}$ phases is known to depend on the oxygen content (e.g., [27]), detailed neutron diffraction studies are necessary to determine exact effects of excess oxygen on the structure of Pr_2NiO_4-based solid solutions. Nevertheless, whatever the mechanism of structural changes, the XRD results confirm that the K_2NiF_4-type phases are stable at moderate oxygen chemical potentials.

Figure 12 compares the electrical properties of Pr_2NiO_4-based materials in the $p(O_2)$ range where the layered K_2NiF_4 phases exist, at 1223 K. In these conditions, $Pr_2NiO_{4+\delta}$ possesses a higher conductivity and a lower thermopower compared to $Pr_2Ni_{0.9}Fe_{0.1}O_{4+\delta}$ and $Pr_2Ni_{0.8}Cu_{0.2}O_{4+\delta}$, probably due to hole trapping on iron cations and lower

Table 2 Example of reproducibility of the oxygen permeation fluxes through 1.00 mm thick $Pr_2NiO_{4+\delta}$ membrane at 1223 K after measurements at different temperatures (p_2=0.21 atm).

Thermal prehistory	p_1, atm	$j\times10^8$, mol×s^{-1}×cm^{-2}
After testing at 1223 K for 260 h	0.073	7.26
	0.047	9.97
	0.025	13.75
After testing at 1073–1123 K for 83 h	0.025	13.59
After subsequent testing at 1223 K for 41 h	0.073	7.55
	0.047	10.23

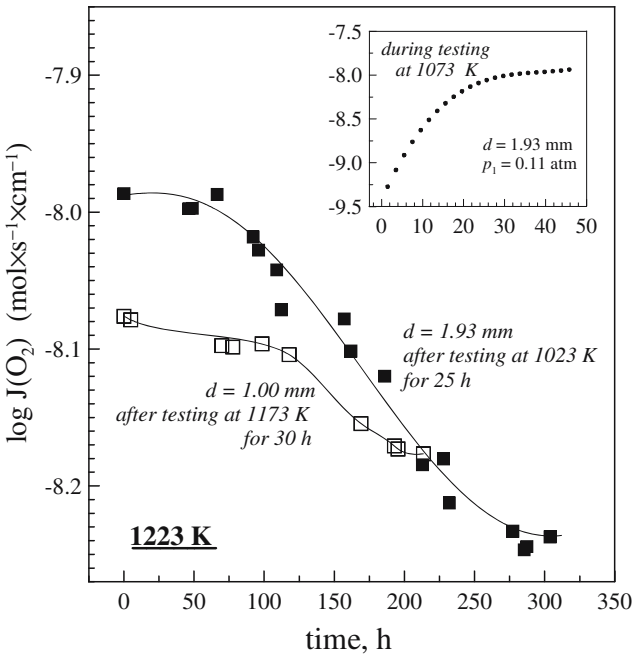

Fig. 15 Examples of the time dependences of the oxygen permeability of $Pr_2NiO_{4+\delta}$ ceramics at 1223 K after testing at lower temperatures. The permeate-side oxygen pressures are 0.036±0.002 and 0.027±0.03 atm for the 1.00 and 1.93 mm thick membranes, respectively. The inset illustrates equilibration processes at 1073 K after cooling

charge-carrier concentration in the Cu-containing phase. Despite such differences, however, all materials exhibit tendency to a plateau-like behavior at moderate $p(O_2)$ values. Further reduction leads to a drastic irreversible decrease in the conductivity, indicating phase decomposition into the binary metal oxides as confirmed by XRD. The approximate stability limits of the K_2NiF_4-type phases are marked in Fig. 12 by arrows.

Figure 13 summarizes the low-$p(O_2)$ boundaries estimated by the measurements of total conductivity and Seebeck coefficient. The decomposition of $Pr_2NiO_{4+\delta}$ occurs at oxygen chemical potentials higher than the stability limit of $La_2NiO_{4+\delta}$ [28]. This trend well corresponds to literature data on other K_2NiF_4-type phases (e.g., [29] and references therein). In particular, thermodynamic stability of rare-earth cuprates with K_2NiF_4 structure also decreases with decreasing A-site cation radius [29]. Doping of $Pr_2NiO_{4+\delta}$ with either iron or copper promotes phase decomposition in reducing atmospheres.

The low-$p(O_2)$ stability limit of $Pr_2NiO_{4+\delta}$ is close to the Ni/NiO boundary [30] at 1173–1223 K, but shifts towards higher oxygen partial pressures when temperature decreases (Fig. 13). This suggests a change in the decomposition mechanism and explains the observed deviations from the linear van't Hoff dependence, log $p(O_2)$ vs. $1/T$. Apparently, at high temperatures the decomposition of $Pr_2NiO_{4+\delta}$ occurs via formation of praseodymium oxide and metallic nickel. At temperatures below 1150 K, the reduction should result in the binary oxides mixture, thus indicating a decrease in the thermodynamic stability of $Pr_2NiO_{4+\delta}$ compared to other phases of ternary Pr–Ni–O system, in correlation with the behavior observed in oxidizing environments.

3.4 Oxygen permeation

Figure 14 presents the steady-state oxygen permeation fluxes through dense $La_2NiO_{4+\delta}$ and $Pr_2NiO_{4+\delta}$ membranes at 1173–1223 K. The values of specific oxygen permeability, $J(O_2)$, were calculated from the permeation flux density j as [31]:

$$J(O_2) = jd \times \left[\ln\frac{p_2}{p_1}\right]^{-1} \quad (2)$$

where d is the membrane thickness. The data on praseodymium nickelate corresponds to the start of measurements, without cooling down to lower temperatures. For both $Pr_2NiO_{4+\delta}$ and $La_2NiO_{4+\delta}$, the permeation fluxes decrease with increasing membrane thickness, whilst the values of specific oxygen permeability demonstrate an opposite trend. Such behavior indicates that the overall oxygen transport is determined by two factors, namely the bulk ionic conduction and surface exchange kinetics [10, 18]. A significant influence of the interfacial exchange processes

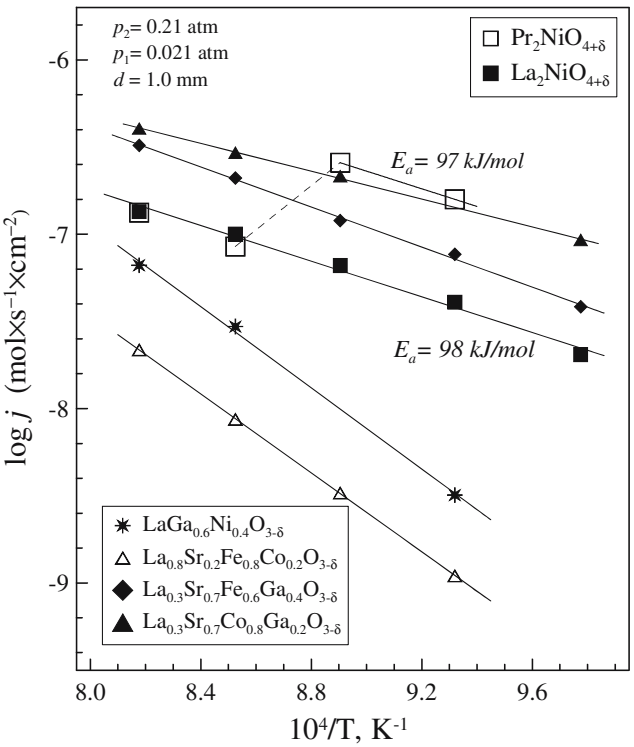

Fig. 16 Temperature dependence of steady-state oxygen permeation fluxes through $Pr_2NiO_{4+\delta}$ and $La_2NiO_{4+\delta}$ under a fixed oxygen chemical potential gradient. The data on selected perovskite-type mixed conductors [34–36] are shown for comparison

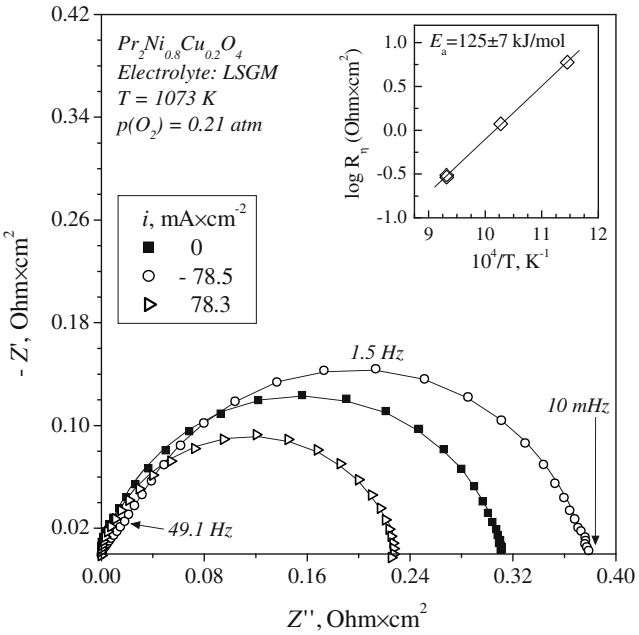

Fig. 17 Examples of the electrode impedance spectra of porous $Pr_2Ni_{0.8}Cu_{0.2}O_{4+\delta}$ layer in contact with LSGM solid electrolyte, at 1073 K in air. *Solid lines* show the fitting results, with an equivalent circuit comprising the resistance and constant-phase element connected in parallel. *Inset* shows the temperature dependence of electrode polarization resistance under open-circuit conditions

on oxygen permeation is typical for most nickelate-based materials [1, 3, 10].

The permeation fluxes through as-prepared $Pr_2NiO_{4+\delta}$ ceramics are apparently higher compared to $La_2NiO_{4+\delta}$ at 1173–1223 K. This seems to agree with literature data [5]. Also, although $Pr_2NiO_{4+\delta}$ is already metastable at 1173 K in air (Fig. 5), XRD inspection of the membranes after testing at 1173–1223 K did not reveal secondary phases; the permeability of as-prepared membranes at 1173 K was essentially time-independent. The kinetic stabilization of K_2NiF_4-type nickelate might result from the presence of oxygen chemical potential gradient in the course of measurements, when the permeate-side oxygen pressure is lower than atmospheric. At the same time, the XRD analysis cannot exclude possible traces of $Pr_4Ni_3O_{10-\delta}$ and praseodymium oxide formed at the grain boundaries during heating of the as-prepared membranes. After testing at lower temperatures, a slow degradation was observed at 1223 K (Fig. 15). The resultant permeation fluxes, independent of time during 100–150 h after the relaxation period, became very similar to those of $La_2NiO_{4+\delta}$ (Fig. 16). Such a decrease cannot be attributed to membrane cracking, which should lead to a higher permeability. Furthermore, after temperature cycling, the oxygen permeation fluxes at 1223 K were reproducible with an accuracy of 5–7%; one example is given in Table 2.

Decreasing temperature down to 1073–1123 K resulted in a slow increase in the oxygen permeability, as illustrated by the inset in Fig. 15. The time necessary for stabilization was as long as 200–300 h. These processes can be undoubtedly ascribed to the partial decomposition in $Pr_4Ni_3O_{10-\delta}$ and PrO_x, confirmed by XRD. Although no systematic information on the ionic transport properties of the Ruddlesden–Popper type $Pr_{n+1}Ni_nO_{3n+1}$ series is found in literature, the data on isostructural $(La,Sr)_{n+1}(Fe,Co)_nO_{3n+1}$ system [32] suggest that increasing the number of perovskite blocks (n) should increase oxygen diffusivity; $Pr_4Ni_3O_{10-\delta}$ is thus expected to possess a higher ionic conductivity compared to $Pr_2NiO_{4+\delta}$. A significant level of mixed ionic–electronic conductivity is also known for praseodymium oxide [33]. After achieving a steady state at 1073–1123 K, the oxygen permeability of $Pr_2NiO_{4+\delta}$ ceramics becomes four to five times higher than that of $La_2NiO_{4+\delta}$ (Fig. 16). The apparent activation energy (E_a) remains essentially unchanged, suggesting that the ionic transport mechanisms are still similar. For comparison, the E_a values in the intermediate-temperature range are 98 kJ/mol for single-phase $La_2NiO_{4+\delta}$ and 97 kJ/mol for multiphase $Pr_2NiO_{4+\delta}$ ceramics.

These results show, in particular, that the fast tracer diffusion and oxygen surface exchange of $Pr_2NiO_{4+\delta}$ ceramics at temperatures below 1100 K [5] may be contributed by $Pr_4Ni_3O_{10-\delta}$ and PrO_x, formed on partial decomposition of the K_2NiF_4-type praseodymium nickelate. When temperature is close to the phase transition or higher, the levels of ionic transport in $Pr_2NiO_{4+\delta}$ and

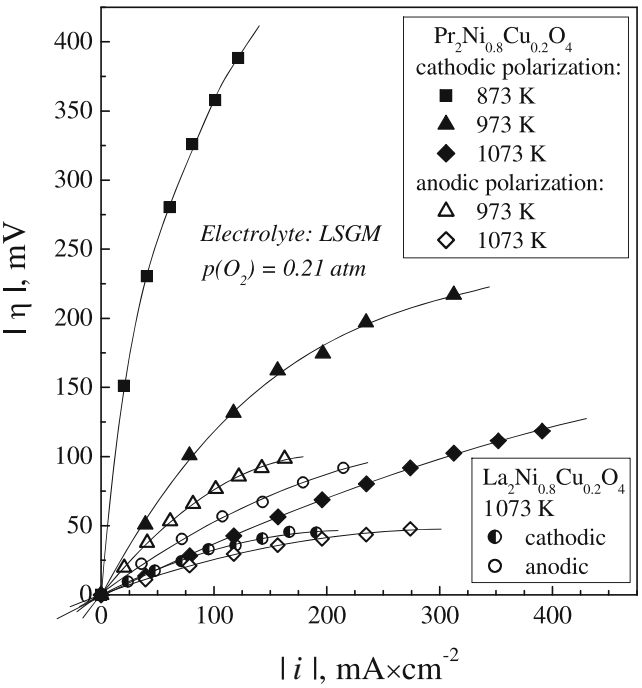

Fig. 18 Comparison of the cathodic and anodic polarization curves of porous $Pr_2Ni_{0.8}Cu_{0.2}O_{4+\delta}$ and $La_2Ni_{0.8}Cu_{0.2}O_{4+\delta}$ electrodes in contact with LSGM solid electrolyte

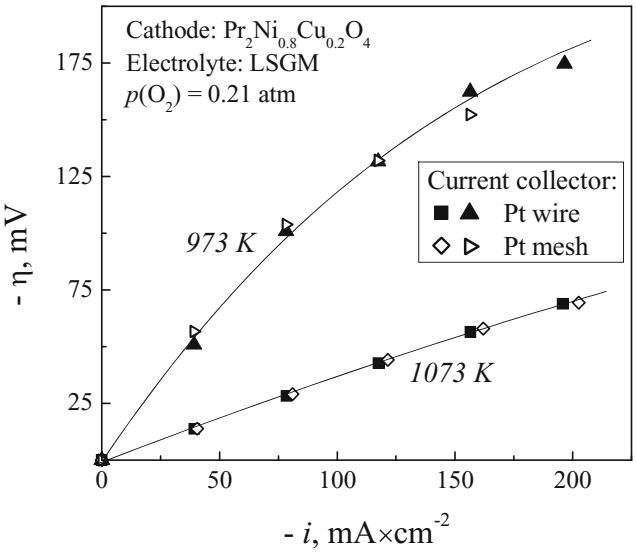

Fig. 19 Current density dependencies of the cathodic overpotentials for two similar $Pr_2Ni_{0.8}Cu_{0.2}O_{4+\delta}$ electrodes, measured using Pt wire or Pt gauze current collectors

$La_2NiO_{4+\delta}$ are similar (Fig. 16), as observed by the authors [5]. Another necessary comment is that below 1173 K, the partly decomposed $Pr_2NiO_{4+\delta}$ ceramics exhibits a very high level of the oxygen permeability. The oxygen fluxes through praseodymium nickelate membranes are still lower than those through most permeable materials such as $Sr(Co,Fe)O_{3-\delta}$ perovskites [18], but comparable to $La_{0.3}Sr_{0.7}Co_{0.8}Ga_{0.2}O_{3-\delta}$ [36].

3.5 Electrochemical behavior of $Pr_2Ni_{0.8}Cu_{0.2}O_{4+\delta}$ electrodes

As for $La_2Ni_{0.8}Cu_{0.2}O_{4+\delta}$ [10], the impedance spectra of porous $Pr_2Ni_{0.8}Cu_{0.2}O_{4+\delta}$ electrodes in contact with LSGM electrolyte consist of a single arc (Fig. 17). The Arrhenius plot of the electrode polarization resistance (inset in Fig. 17) under open-circuit conditions in air is almost linear, with an activation energy of 125±7 kJ/mol. However, in contrast to $La_2Ni_{0.8}Cu_{0.2}O_{4+\delta}$, both ohmic and polarization resistances of $Pr_2Ni_{0.8}Cu_{0.2}O_{4+\delta}$ layers were found strongly dependent on the electrode potential, increasing under cathodic polarization when prolonged relaxation processes were observed. At fixed current density, the steady-state cathodic overpotentials of praseodymium nickelate-based layers are considerably higher than anodic; $La_2Ni_{0.8}Cu_{0.2}O_{4+\delta}$ exhibits an opposite tendency (Fig. 18).

This behavior correlates, again, with the phase transformation starting at 1073 K (Fig. 5c). The partial decomposition of $Pr_2Ni_{0.8}Cu_{0.2}O_{4+\delta}$ increases electronic conductivity (Figs. 6 and 8); the ionic conduction is also expected to increase (Fig. 16). The former factor may contribute to increasing ohmic resistance under cathodic conditions when the oxygen chemical potential is reduced, thus inducing transition into the K_2NiF_4-type phase. At the same time, testing of $Pr_2Ni_{0.8}Cu_{0.2}O_{4+\delta}$ electrodes with different current collectors showed that the influence of electronic transport processes on oxygen reduction kinetics is negligible. As an example, Fig. 19 presents the current–overpotential curves for two cathodes, where the current was collected by a single Pt wire (thickness of 0.5 mm) and a Pt gauze (wire thickness of 0.1 mm, spacing of approximately 0.4 mm). The overpotentials are equal within the limits of experimental uncertainty, which indicates an absence of the current constriction effects [37]. Therefore, the factors responsible for the relatively low anodic overpotentials may be related to increasing ionic transport and exchange currents due to polarization-induced oxidation, promoting the transition into $Pr_4Ni_3O_{10-\delta}$ and PrO_x; the segregation of electrocatalytically active praseodymium oxide phase leads to a substantially higher electrochemical activity of nickelate electrodes [10].

4 Conclusions

Dense ceramics of $Pr_2NiO_{4+\delta}$, $Pr_2Ni_{0.9}Fe_{0.1}O_{4+\delta}$, $Pr_2Ni_{0.8}Cu_{0.2}O_{4+\delta}$ and $La_2NiO_{4+\delta}$ were prepared by the glycine-nitrate process followed by sintering in air at 1573–1673 K, and characterized employing XRD, SEM/EDS, TGA, dilatometry, and the measurements of total conductivity, Seebeck coefficient and oxygen permeability. In oxidizing atmospheres, all Pr_2NiO_4-based materials exhibit an extensive oxygen uptake and decomposition into the Ruddlesden–Popper type $Pr_4Ni_3O_{10}$ and praseodymium oxide phases at temperatures below 1073–1223 K. The transition temperature determined by the oxygen content increases on Cu doping, and decreases when nickel is substituted by Fe cations. At 1173–1223 K when the K_2NiF_4-type praseodymium nickelate is kinetically stable in the ceramic membranes placed under an oxygen partial pressure gradient, the steady-state oxygen permeability of $Pr_2NiO_{4+\delta}$ is similar to $La_2NiO_{4+\delta}$. As for other nickelates, the permeation is limited by both surface exchange and bulk ionic conductivity. The phase changes on cooling lead to considerably higher electronic conductivity and oxygen permeability, which become comparable to the transport properties of perovskite-type cobaltites. However, these changes are associated also with a significant volume expansion, limiting practical applications. The stability of $Pr_2NiO_{4+\delta}$ in reducing atmospheres, estimated from the $p(O_2)$ dependencies of total conductivity and Seebeck coefficient, is lower than that of $La_2NiO_{4+\delta}$, probably due to a smaller size of the A-site cations. Doping with either iron or copper shifts the low-$p(O_2)$ decomposition boundary towards higher oxygen pressures. The porous $Pr_2Ni_{0.8}Cu_{0.2}O_{4+\delta}$ electrodes applied onto LSGM solid

electrolyte exhibit lower anodic overpotentials compared to $La_2Ni_{0.8}Cu_{0.2}O_{4+\delta}$, whereas cathodic reduction decreases their performance. The results suggest that a promising combination of high electronic conductivity and fast ionic transport may be expected for $Pr_4Ni_3O_{10}$-based solid solutions where, however, the Ruddlesden–Popper type phase should be stabilized up to the high temperatures necessary for sintering. This stabilization can be achieved by substitution of nickel with higher-valence cations, such as iron.

Acknowledgements This work was supported by the FCT, Portugal (projects POCI/CTM/59197/2004, SFRH/BPD/15003/2004 and SFRH/BPD/24639/2005), and by the NATO Science for Peace program (project 978002). Experimental assistance and helpful discussions, made by A. Shaula and M. Patrakeev, are gratefully acknowledged.

References

1. B.Vigeland, R.Glenne, T.Breivik, S.Julsrud, Int. Patent Application PCT WO 99/59702 (1999)
2. J.A. Kilner, C.K.M. Shaw, Solid State Ionics **154–155**, 523 (2002)
3. V.V.Kharton, A.P.Viskup, A.V.Kovalevsky, E.N.Naumovich, Solid State Ionics **143**, 337 (2001)
4. E. Boehm, J.M. Bassat, M.C. Steil, P. Dordor, F. Mauvy, J.C. Grenier, Solid State Sci. **5**, 973 (2003)
5. E. Boehm, J.-M. Bassat, P. Dordor, F. Mauvy, J.-C. Grenier, Ph. Stevens, Solid State Ionics **176**, 2717 (2005)
6. V.V. Vashook, I.I. Yushkevich, L.V. Kokhanovsky, L.V. Makhnach, S.P. Tolochko, I.F. Kononyuk, H. Ullmann, H. Altenburg, Solid State Ionics **119**, 23 (1999)
7. P. Odier, Ch. Allançon, J.M. Bassat, J. Solid State Chem. **153**, 381 (2000)
8. D.C. Zhu, X.Y. Xu, S.J. Feng, W. Liu, C.S. Chen, Catal. Today **82**, 151 (2003)
9. S. Miyoshi, T. Furuno, H. Matsumoto, T. Ishihara, Solid State Ion. **177**, 2269 (2006)
10. V.V. Kharton, E.V. Tsipis, A.A. Yaremchenko, J.R. Frade, Solid State Ion. **166**, 327 (2004)
11. S.J. Skinner, J.A. Kilner, Solid State Ion. **135**, 709 (2000)
12. A.A. Yaremchenko, A.A. Valente, V.V. Kharton, E.V. Tsipis, J.R. Frade, E.N. Naumovich, J. Rocha, F.M.B. Marques, Catal. Letters **91**, 169 (2003)
13. C. Allançon, A. Gonthier-Vassal, J.M. Bassat, J.P. Loup, P. Odier, Solid State Ion. **74**, 239 (1994)
14. L.A. Chick, L.R. Pederson, G.D. Maupin, J.L. Bates, L.E. Thomas, G.L. Exarhos, Mater. Lett. **10**, 6 (1990)
15. J. Rodriguez-Carvajal, Physica B. **192**, 55 (1993)
16. E.N. Naumovich, M.V. Patrakeev, V.V. Kharton, A.A. Yaremchenko, D.I. Logvinovich, F.M.B. Marques, Solid State Sci. **7**, 1353 (2005)
17. I.A. Leonidov, V.L. Kozhevnikov, E.B. Mitberg, M.V. Patrakeev, V.V. Kharton, F.M.B. Marques, J. Mater. Chem. **11**, 1201 (2001)
18. V.V. Kharton, V.N. Tikhonovich, Li Shuangbao, E.N. Naumovich, A. V. Kovalevsky, A.P. Viskup, I.A. Bashmakov, A.A. Yaremchenko, J. Electrochem. Soc. **145**, 1363 (1998)
19. E.V. Tsipis, V.V. Kharton, I.A. Bashmakov, E.N. Naumovich, J.R. Frade, J. Solid State Electrochem. **8**, 674 (2004)
20. J. Rodríguez-Carvajal, M.T. Fernández-Díaz, J.L. Martínez, J. Phys.: Condens. Matter **3**, 3215(1991)
21. D.J. Buttrey, J.D. Sullivan, G. Shirane, K. Yamada, Phys. Rev. B **42**, 3944 (1990)
22. M. Medarde, A. Fontaine, J.L. Garcia-Munoz, J. Rodriguez-Carvajal, M. de Santis, M. Sacchi, G. Rossi, P. Lacorre, Phys. Rev. B **46**, 14975 (1992)
23. C. Allançon, P. Odier, J.M. Bassat, J.P. Loup, J. Solid State Chem. **131**, 167 (1997)
24. J.M. Bassat, C. Allançon, P. Odier, J.P. Loup, M. Deus Carvalho, A. Wattiaux, Eur. J. Solid State Inorg. Chem. **35**, 173 (1998)
25. Ph. Lacorre, J. Solid State Chem. **97**, 495 (1992)
26. Z. Zhang, M. Greenblatt, J. Solid State Chem. **117**, 236 (1995)
27. M.T. Fernández-Díaz, J.L. Martínez, J. Rodríguez-Carvajal, Solid State Ionics **63–65**, 902 (1993)
28. M. Zinkevich, F. Aldinger, J. Alloys Compd. **375**, 147 (2004)
29. V.V. Kharton, A.A. Yaremchenko, E.N. Naumovich, J. Solid State Electrochem. **3**, 303 (1999)
30. G.G. Charette, S.N.Flengas, J. Electrochem. Soc. **115**, 796 (1968)
31. H.H. Möbius, in *Ext. Abst. 37th Meeting of International Society of Electrochemistry*, Vilnius, Lithuania (1986), vol. 1, p. 136
32. A. Manthiram, F. Prado, T. Armstrong, Solid State Ion. **152–153**, 647 (2002)
33. P. Huang, A. Petric, in *Ionic and Mixed Conducting Ceramics III*, ed. By T.A. Ramanarayanan (The Electrochemical Society, Pennington, NJ, 1998) PV97-24, p. 396
34. A.A. Yaremchenko, V.V. Kharton, E.N. Naumovich, D.I. Shestakov, V.F. Chukharev, A.V. Kovalevsky, A.L. Shaula, J.R. Frade, F.M.B. Marques, Solid State Ion. **177**, 549 (2006)
35. V.V. Kharton, A.A. Yaremchenko, A.P. Viskup, M.V. Patrakeev, I. A. Leonidov, V.L. Kozhevnikov, F.M. Figueiredo, A.L. Shaulo, E. N. Naumovich, F.M.B. Marques, J. Electrochem. Soc. **149**, E125 (2002)
36. V.V. Kharton, E.V. Tsipis, I.P. Marozau, A.A. Yaremchenko, A.A. Valente, A.P. Viskup, J.R. Frade, E.N. Naumovich, J. Rocha, J. Solid State Electrochem. **9**, 10 (2005)
37. K. Sasaki, J.-P. Wurth, R. Gschwend, M. Gödickemeier, L.J. Gauckler, J. Electrochem. Soc. **143**, 530 (1996)